Supporting Information

Orthogonal Di-Spiro Skeleton Engineering on Suppressing π-π Stacking and Spectral Broadening for High-Performance Narrowband Electroluminescence

Hao-Ze Li[a], Yu-Tao Yang[b], Yi-Cheng Zhao[b], Feng-Ming Xie[b,*], Jian-Xin Tang[c,*], Yan-Qing Li[a,*]

[a] School of Physics and Electronic Science, East China Normal University Shanghai 200062 (P. R. China)

[b] Institute of Functional Nano & Soft Materials (FUNSOM), Soochow University, Suzhou, Jiangsu 215123 (P. R. China)

[c] Macao Institute of Materials Science and Engineering (MIMSE), Macau University of Science and Technology, Taipa, Macau SAR 999078 (P. R. China)

* Corresponding author.

E-mail address: fmxie@suda.edu.cn (F.-M. Xie), jxtang@must.edu.mo (J.-X. Tang) yqli@phy.ecnu.edu.cn (Y.-Q. Li)

1. Synthesis and characterization

All the reagents and solvents were obtained from commercial sources and directly used without any further purification. ^{1}H NMR and ^{13}C NMR were recorded with Germany Bruker AVANCE III type NMR Spectrometer in $CDCl_3$ solution. Matrix-assisted laser desorption/ionization time-of-flight (MALDI-TOF) mass spectroscopy was acquired on an UltrafleXtreme MALDI-TOF mass spectrometer with a 1 KHz smart beam-II laser.

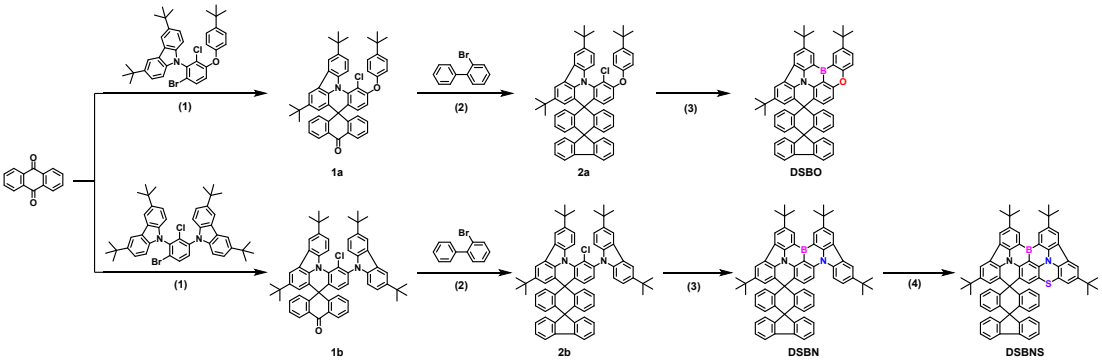

Scheme S1. The synthetic route of **DSBO**, **DSBN** and **DSBNS**. (1), (2) = i) THF, n-BuLi; ii) AcOH, HCl; (3) = i) mesitylene, t-BuLi; ii) BBr_3; iii) DIPEA; (4) I_2, S, oDCB.

1.1 Synthesis of 3',6'-di-*tert*-butyl-11'-(4-(*tert*-butyl)phenoxy)-12'-chloro-10*H*-spiro[anthracene-9,8'-indolo[3,2,1-de]acridin]-10-one (**1a**)

Under a nitrogen atmosphere, compound 9-(6-bromo-3-(4-(*tert*-butyl)phenoxy)-2-chlorophenyl)-3,6-di-*tert*-butyl-9*H*-carbazole (3.00 g, 4.88 mmol) was dissolved in 60 mL of tetrahydrofuran in a 200 mL Schlenk reaction flask. The solution was cooled to -78 °C, and 2.20 M of n-butyllithium (2.66 mL, 5.85 mmol) was added dropwise with a syringe. After stirring for 2 hours, anthracene-9,10-dione (2.03 g, 9.75 mmol)

was added. The reaction was allowed to proceed overnight, and then 5 mL of water was added to quench the reaction. The solution was evaporated to dryness under reduced pressure. The resulting solid was dissolved in 80 mL of glacial acetic acid, heated to 120 ℃, and stirred for half an hour. Subsequently, 9 mL of hydrochloric acid (36%) was added, and the reaction was allowed to proceed for 24 hours. The reaction mixture was poured into ice-cold water, resulting in the precipitation of a large amount of solid. The solid was filtered and separated by silica gel column chromatography (DCM : *n*-H = 1 : 5) to obtain a white solid, compound **1a** (1.86 g, 2.56 mmol) with a yield of 52.34%. MALDI-TOF-MS (m/z) of $C_{50}H_{46}ClNO_2$ for $[M]^+$: calcd. 727.322; found, 727.233.

1.2 Synthesis of 3",6"-di-*tert*-butyl-11"-(4-(*tert*-butyl)phenoxy)-12"-chlorodispiro[fluorene-9,9'-anthracene-10',8"-indolo[3,2,1-*de*]acridine] (**2a**)

Under a nitrogen atmosphere, compound 2-bromo-1,1'-biphenyl (1.91 g, 8.25 mmol) was dissolved in 60 mL of tetrahydrofuran in a 200 mL Schlenk reaction flask. The solution was cooled to -78 ℃, and 2.20 M of n-butyllithium (4.50 mL, 9.90 mmol) was added dropwise with a syringe. After stirring for 2 hours, compound **1a** (3.00 g, 4.12 mmol) was added. The reaction was allowed to proceed overnight, and then 5 mL of water was added to quench the reaction. The solution was evaporated to dryness under reduced pressure. The resulting solid was dissolved in 80 mL of glacial acetic acid, heated to 120 ℃, and stirred for half an hour. Subsequently, 9 mL of hydrochloric acid (36%) was added, and the reaction was allowed to proceed for 24 hours. The

reaction mixture was poured into ice-cold water, resulting in the precipitation of a large amount of solid. The solid was filtered and separated by silica gel column chromatography (DCM : *n*-H = 1 : 10) to obtain a white solid, compound **2a** (2.37 g, 2.74 mmol) with a yield of 42.48%. MALDI-TOF-MS (m/z) of $C_{62}H_{54}ClNO$ for $[M]^+$: calcd. 863.389; found, 863.082.

1.3 Synthesis of **DSBO**

Compound **2a** (2.89 g, 3.35 mmol) was dissolved in dry mesitylene solution (50 mL) under nitrogen atmosphere and cooled to -40 °C. Then 1.30 M of *t*-butyllithium (5.20 mL, 6.76 mmol) was slowly added into the reaction mixture. The reaction mixture was slowly warmed to room temperature and stirred at 90 °C for 3 hours. After that, 1.00 M of BBr_3 (7.00 mL, 7.00 mmol) was slowly added at -20 °C, and then the mixture was stirred at room temperature for 3 hours. After addition of *N*,*N*-diisopropylethylamine (DIPEA, 5.00 mL) at 0 °C, the reaction mixture was further stirred at 170 °C for 24 hours. An aqueous solution of sodium acetate was added to the reaction mixture. Then the resulting mixture was extracted by dichloromethane for three times. The organic phase was dried over anhydrous $MgSO_4$, filtered and concentrated under reduced pressure. The crude product was further purified by silica gel column chromatography (DCM : *n*-H = 1 : 10) to obtain a yellow solid, compound **DSBO** (0.61 g, 0.73 mmol) with a yield of 21.68%. ^{1}H NMR (400 MHz, $CDCl_3$) δ 9.02 (t, J = 1.9 Hz, 1H), 8.93 (t, J = 2.2 Hz, 1H), 8.59 (t, J = 1.8 Hz, 1H), 8.08 (t, J = 1.6 Hz, 1H), 7.93 (dd, J = 7.5, 5.1 Hz, 2H), 7.77 (ddd, J = 8.8, 2.6, 1.1 Hz, 1H), 7.57 – 7.41 (m,

5H), 7.39 – 7.25 (m, 4H), 7.12 (dd, J = 8.6, 1.5 Hz, 1H), 7.02 (dt, J = 7.5, 2.0 Hz, 2H), 6.85 – 6.76 (m, 4H), 6.49 – 6.39 (m, 2H), 1.69 (d, J = 1.7 Hz, 9H), 1.55 (d, J = 1.5 Hz, 9H), 1.37 (d, J = 1.7 Hz, 9H). ^{13}C NMR (400 MHz, $CDCl_3$) δ 158.76, 157.91, 157.82, 157.51, 147.59, 145.03, 143.05, 140.84, 140.36, 140.02, 135.95, 134.31, 132.60, 132.13, 131.87, 131.24, 130.64, 130.31, 129.46, 128.75, 128.35, 128.11, 127.71, 127.57, 127.24, 126.75, 125.63, 125.59, 125.32, 124.92, 123.96, 123.52, 123.05, 120.30, 120.15, 117.98, 116.67, 109.43, 77.24, 58.10, 49.71, 35.56, 35.54, 34.57, 32.38, 32.15, 31.61. MALDI-TOF-MS (m/z) of $C_{62}H_{52}BNO$ for $[M]^+$: calcd. 837.414; found, 837.322.

1.4 Synthesis of 3',6'-di-*tert*-butyl-12'-chloro-11'-(3,6-di-*tert*-butyl-9*H*-carbazol-9-yl)-10*H*-spiro[anthracene-9,8'-indolo[3,2,1-*de*]acridin]-10-one (**1b**)

Compound **1b** was prepared by the same procedure with compound **1a** excepting using the 9,9'-(4-bromo-2-chloro-1,3-phenylene)bis(3,6-di-*tert*-butyl-9*H*-carbazole) (3.00 g, 4.03 mmol) to get the white solid compound **1b** (2.16 g, yield: 62.54%). MALDI-TOF-MS (m/z) of $C_{60}H_{57}ClN_2O$ for $[M]^+$: calcd. 856.416; found, 856.006.

1.5 Synthesis of 3'',6''-di-*tert*-butyl-12''-chloro-11''-(3,6-di-*tert*-butyl-9*H*-carbazol-9-yl)dispiro[fluorene-9,9'-anthracene-10',8''-indolo[3,2,1-*de*]acridine] (**2b**)

Compound **2b** was prepared by the same procedure with compound **2a** excepting using the compound **1b** (3.00 g, 3.50 mmol) to get the white solid compound **2b** (3.34 g, yield: 52.18%). MALDI-TOF-MS (m/z) of $C_{72}H_{65}ClN_2$ for $[M]^+$: calcd. 992.484; found, 991.998.

1.6 Synthesis of **DSBN**

Compound **DSBN** was prepared by the same procedure with compound **DSBO** excepting using the compound **2b** (3.16 g, 3.18 mmol). The crude product was further purified by silica gel column chromatography (DCM : *n*-H = 1 : 10) to obtain a orange solid, compound **DSBN** (1.47 g, 1.52 mmol) with a yield of 47.82%. ^{1}H NMR (400 MHz, $CDCl_3$) δ 9.21 (dd, J = 3.6, 1.7 Hz, 2H), 8.62 (d, J = 1.5 Hz, 1H), 8.51 (d, J = 1.8 Hz, 1H), 8.33 – 8.26 (m, 2H), 8.19 (d, J = 8.8 Hz, 1H), 8.13 (d, J = 1.4 Hz, 1H), 8.02 – 7.97 (m, 2H), 7.73 (d, J = 8.7 Hz, 1H), 7.63 (dd, J = 8.8, 2.1 Hz, 1H), 7.57 – 7.51 (m, 2H), 7.51 – 7.44 (m, 3H), 7.36 – 7.30 (m, 2H), 7.16 – 7.11 (m, 2H), 6.85 (pd, J = 7.0, 1.7 Hz, 4H), 6.53 – 6.46 (m, 2H), 1.74 (d, J = 8.7 Hz, 18H), 1.54 (s, 9H), 1.42 (s, 9H). ^{13}C NMR (400 MHz, $CDCl_3$) δ 157.86, 157.58, 147.47, 145.30, 145.06, 144.73, 143.27, 142.56, 142.02, 140.92, 140.33, 139.62, 138.21, 135.58, 134.27, 132.17, 130.15, 129.76, 128.73, 128.37, 128.11, 127.73, 127.56, 127.29, 126.92, 126.74, 126.23, 125.64, 125.34, 124.47, 124.04, 123.71, 123.21, 122.97, 120.94, 120.30, 120.17, 117.18, 116.55, 113.98, 108.46, 58.14, 49.76, 35.54, 35.16, 34.79, 32.40, 32.18, 32.13, 31.83, 0.01. MALDI-TOF-MS (m/z) of $C_{72}H_{63}BN_2$ for $[M]^+$: calcd. 966.508; found, 966.443.

1.7 Synthesis of **DSBNS**

Under a nitrogen atmosphere, iodine (300 mg, 1.18 mmol), sulfur (1.65 g, 51.75 mmol) and compound **DSBN** (1.00 g, 1.04 mmol) were added into a 100 mL two necked round bottom flask. After 50 mL degassed 1,2-dichlorobenzene (o-DCB) was

added into the flask, the reaction was allowed heating up to reflux and stirred for 4 days. After cooling to room temperature, the reaction mixture was directly concentrated under reduced pressure. The crude product was further purified by silica gel column chromatography (DCM : *n*-H = 1 : 10) to obtain a purple solid, compound **DSBNS** (0.35 g, 0.34 mmol) with a yield of 33.49%. ^{1}H NMR (400 MHz, $CDCl_3$) δ 9.00 (s, 1H), 8.53 (d, J = 1.4 Hz, 1H), 8.33 (s, 1H), 8.06 (d, J = 1.2 Hz, 1H), 7.94 (t, J = 7.9 Hz, 2H), 7.54 – 7.36 (m, 5H), 7.25 (s, 5H), 7.07 (d, J = 8.0 Hz, 2H), 6.94 – 6.76 (m, 5H), 6.45 (d, J = 7.9 Hz, 2H), 1.67 (d, J = 17.9 Hz, 18H), 1.37 (d, J = 10.3 Hz, 18H). ^{13}C NMR (400 MHz, $CDCl_3$) δ 157.82, 157.31, 140.88, 140.29, 132.00, 128.89, 128.35, 127.73, 127.55, 127.39, 126.94, 125.42, 125.26, 120.28, 120.19, 58.04, 32.10. MALDI-TOF-MS (m/z) of $C_{72}H_{61}BN_2S$ for $[M]^+$: calcd. 996.465; found, 996.447.

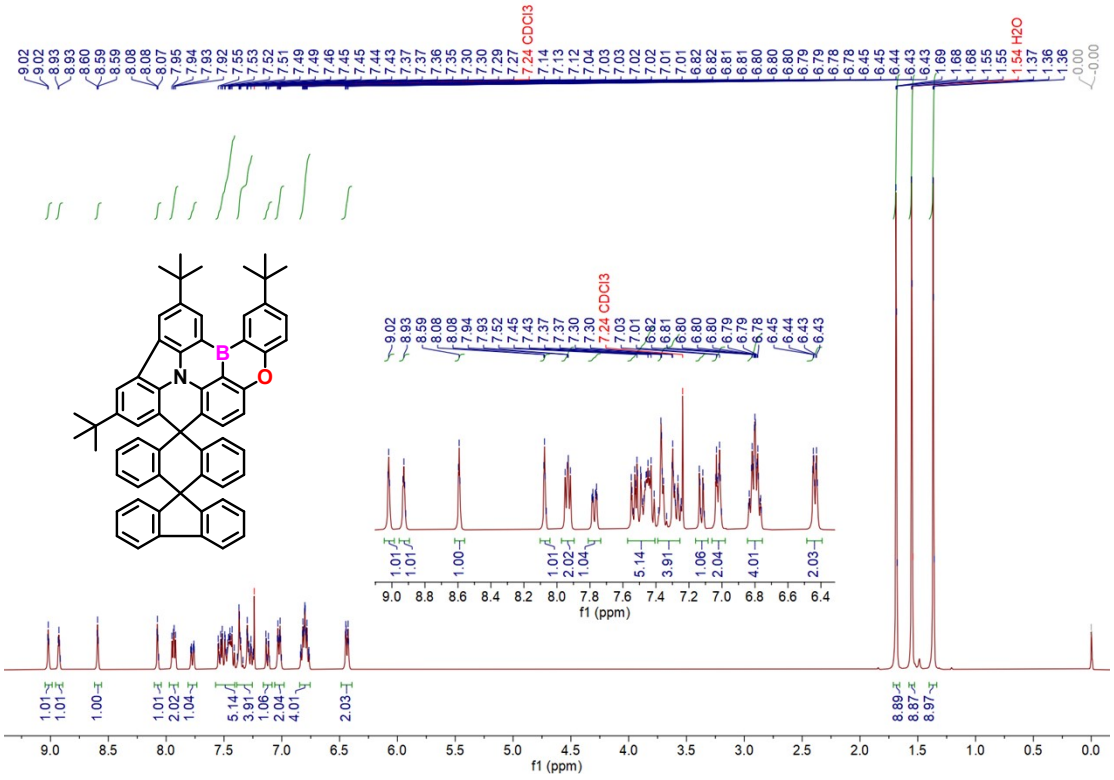

Figure S1. ^{1}H NMR spectrum of DSBO.

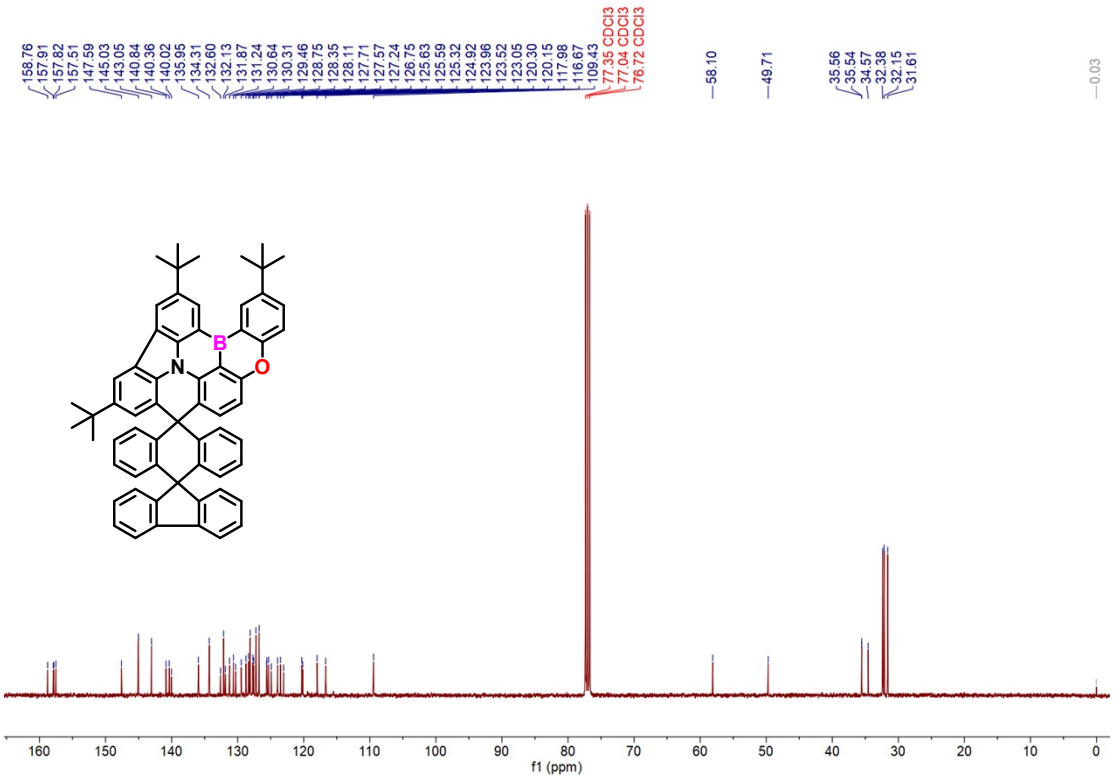

Figure S2. ^{13}C NMR spectrum of DSBO.

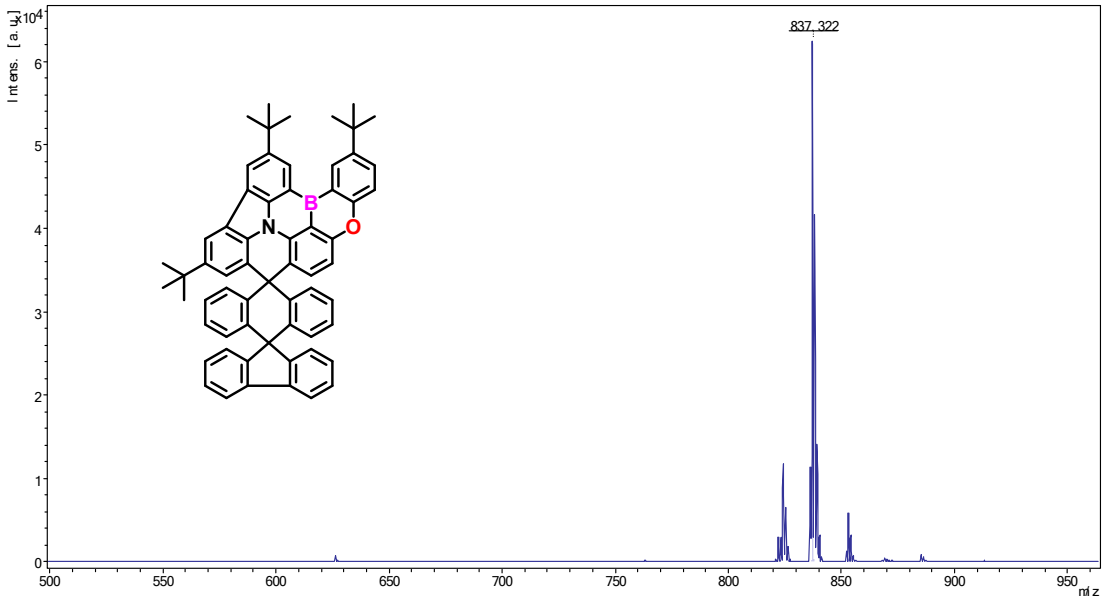

Figure S3. MALDI-TOF MS spectrum of DSBO.

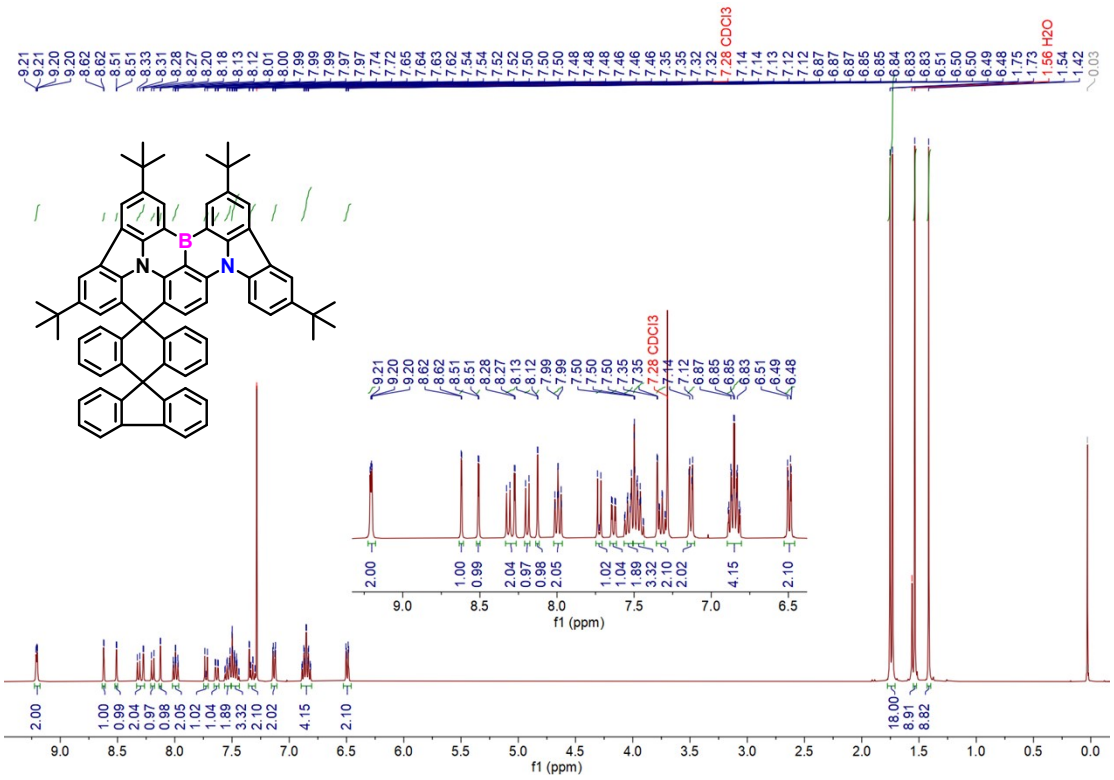

Figure S4. ^{1}H NMR spectrum of DSBN.

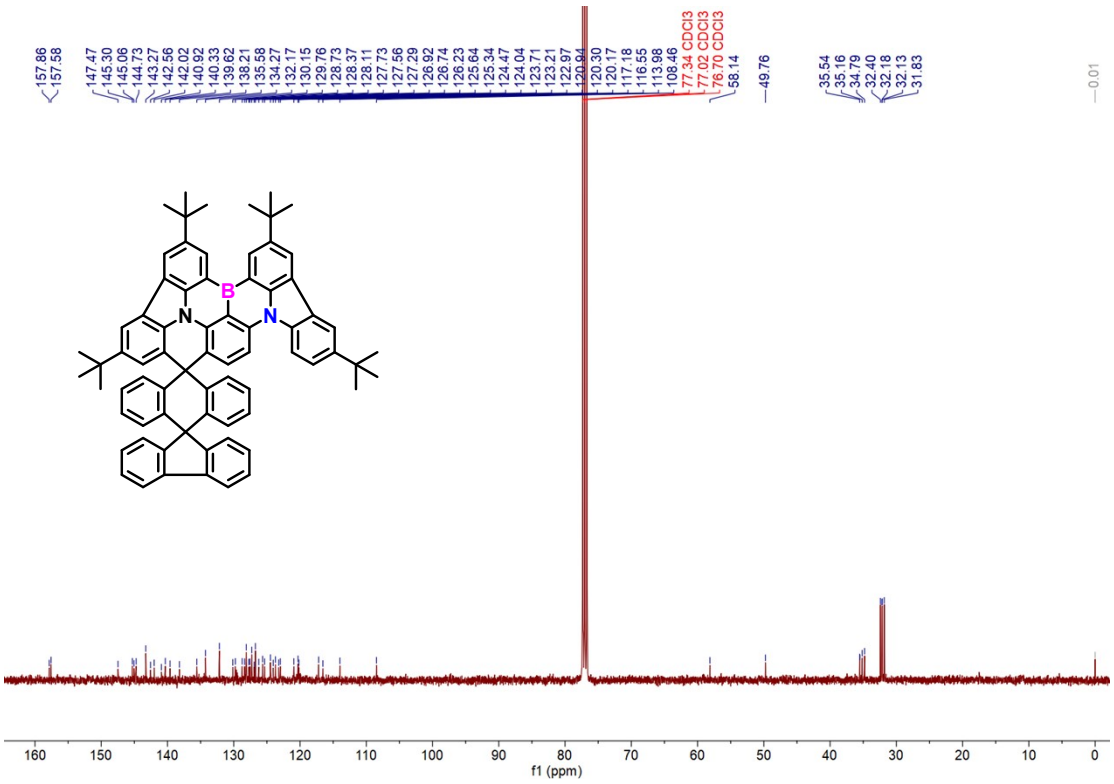

Figure S5. ^{13}C NMR spectrum of DSBN.

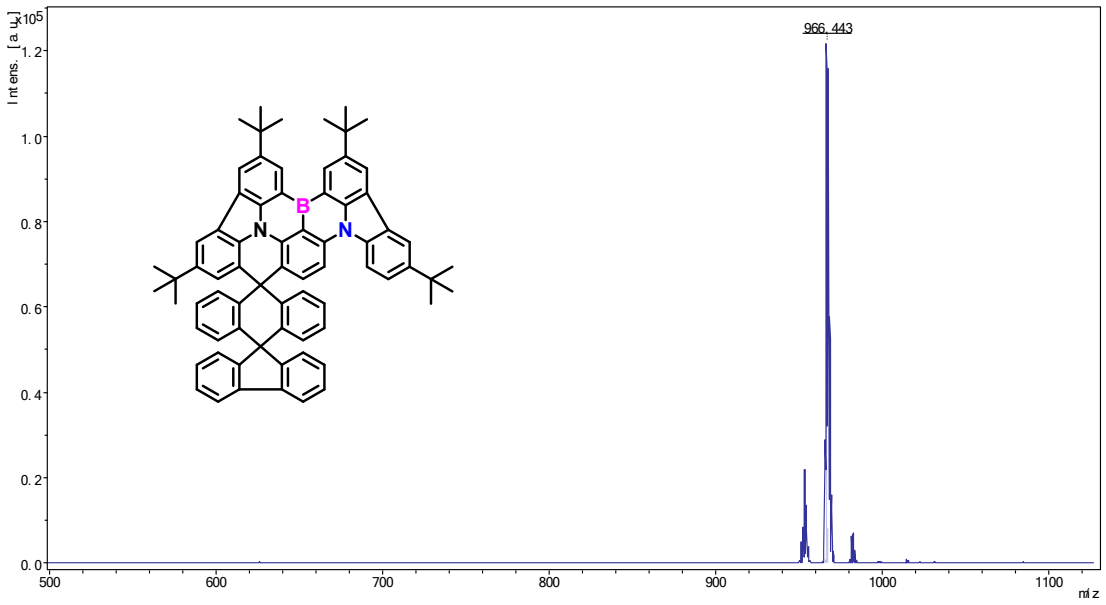

Figure S6. MALDI-TOF MS spectrum of DSBN.

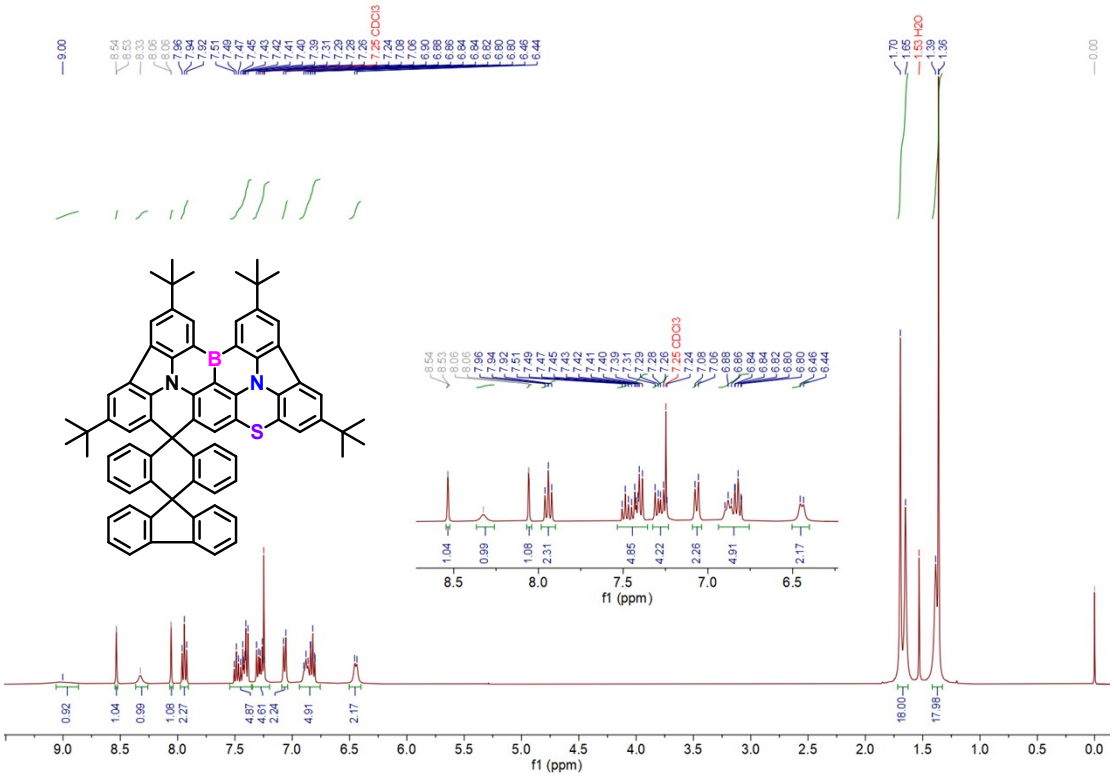

Figure S7. ^{1}H NMR spectrum of DSBNS.

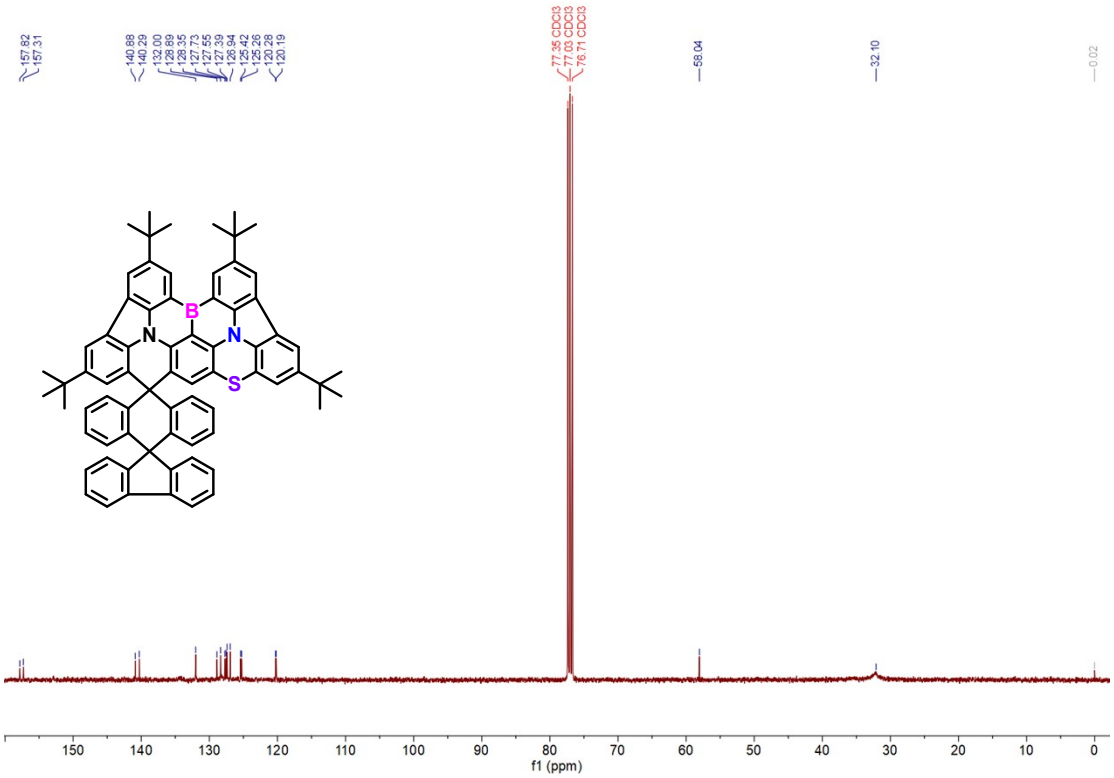

Figure S8. ^{13}C NMR spectrum of DSBNS.

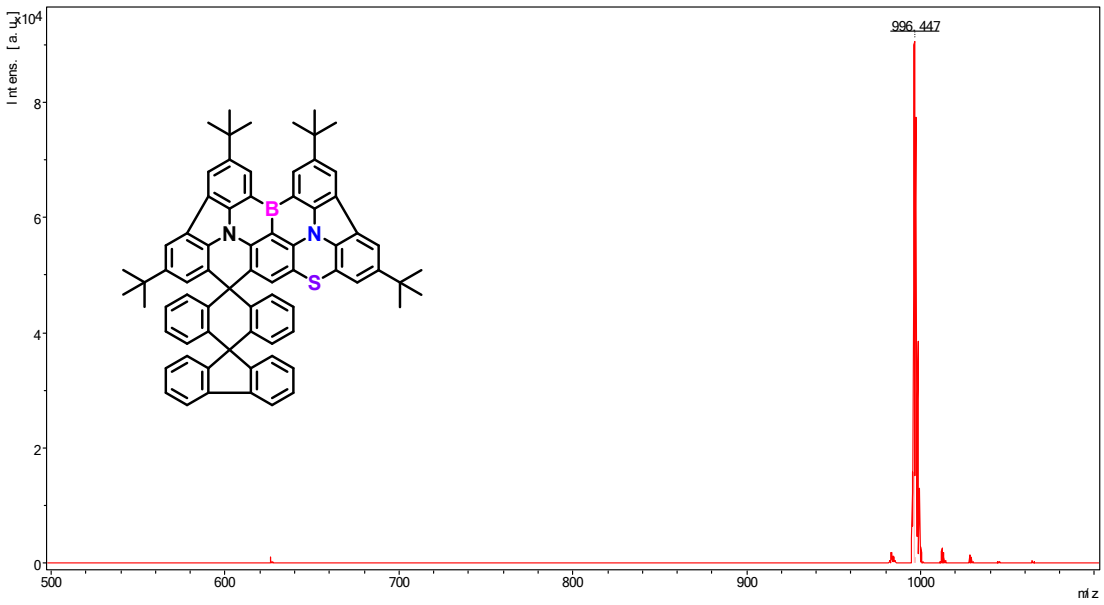

Figure S9. MALDI-TOF MS spectrum of DSBNS.

2. Thermal Characterization

An HCT-2 instrument was employed to analyze thermal gravimetric analysis (TGA) ranging from 25 °C to 800 °C with a heating rate of 10 °C min^{-1} under nitrogen flushing. Differential scanning calorimetry (DSC) was performed from 25 °C to 300 °C at a heating rate of 10 °C min^{-1} under nitrogen flow.

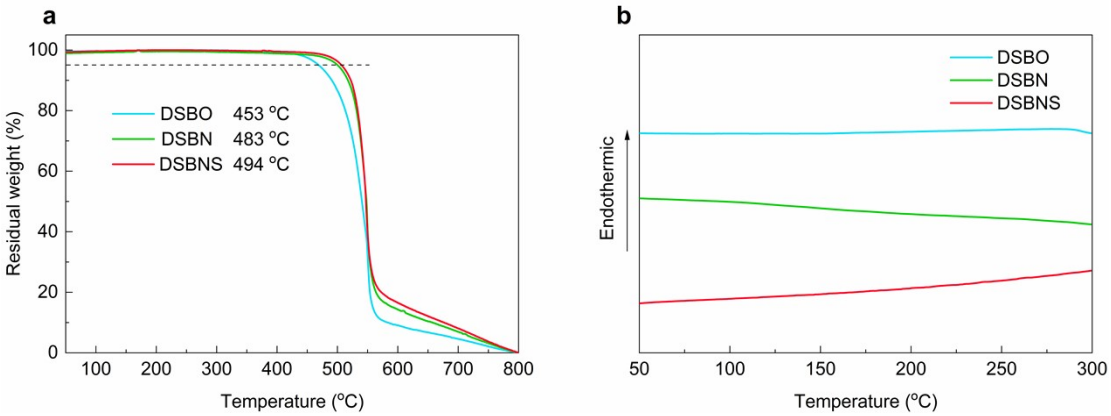

Figure S10. (a) TGA and (b) DSC curves of DSBO, DSBN and DSBNS.

3. Electrochemical Characterization

Cyclic voltammograms (CV) were obtained in dichloromethane at room temperature with a CHI600 electrochemical workstation at 25 °C and a scan speed of 50 mV s^{-1}. The electrochemical oxidation potentials were collected by cyclic voltammetry measurements via a CHI660 electrochemical workstation (Chenhua, China) and ferroceniumferrocene (Fc/Fc^{+}) was used as the internal reference, tetrabutylammonium hexafluorophosphate (0.1 M) was used as the supporting electrolyte. A platinum plate electrode was utilized as the working electrode, a platinum wire was utilized as the counter electrode and Ag/AgCl as reference electrode. The reduction potentials were calculated from $E_{ox} - E_g$, the optical bandgaps (E_g) were estimated from the onset of the absorption spectra.

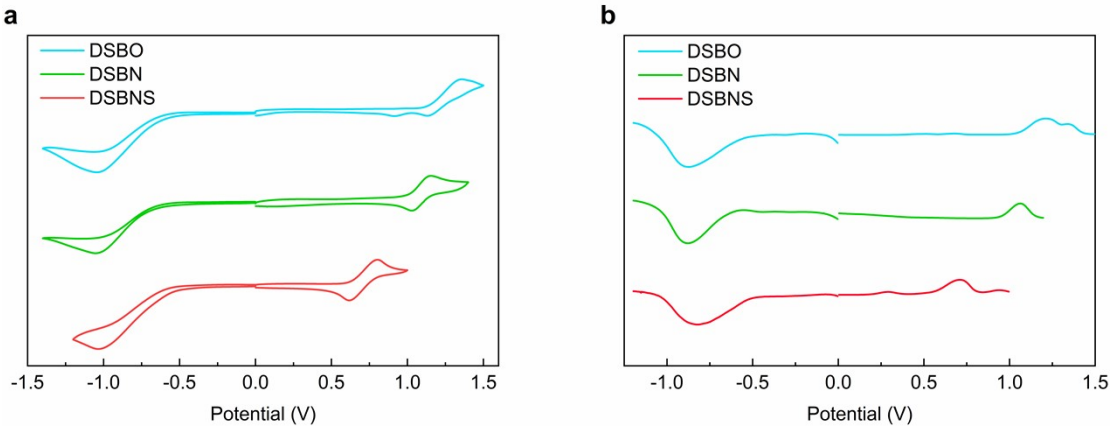

Figure S11. (a) CV and (b) DPV curves of DSBO, DSBN and DSBNS.

4. X-ray crystal structure analysis

Data collections of single crystal X-ray diffraction were performed on a Bruker D8-Venture diffractometer with a Turbo X-ray Source Mo Kα radiation) adopting the direct drive rotating anode technique and a CMOS detector. The data frames were collected using the program APEX2 and processed using the program SAINT routine in APEX2. The structures were solved by direct methods and refined by the full-matrix least squares on F2 using the SHELXTL-2014 program. The SQUEEZE approach was not used in the final refinement. The crystallographic data have been deposited in the Cambridge Crystallographic Data Centre (CCDC) under reference number CCDC: 2464387 (DSBO), 2464390 (DSBN), and 2464393 (DSBNS). The data can be obtained free of charge from the CCDC.

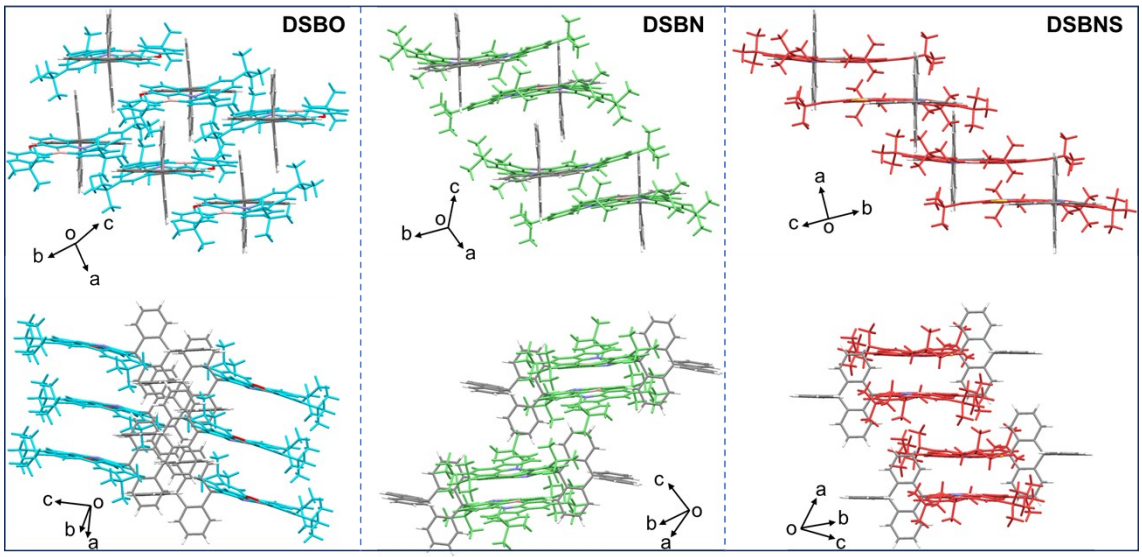

Figure S12. Single-crystal packing diagram of three molecules.

Table S1. Crystal data and structure refinement for **DSBO.**

Compound	DSBO
Empirical formula	$C_{62}H_{52}BNO$
Chemical formula weight	837.85
CCDC number	2464387
Temperature/K	140
Crystal system	monoclinic
Space group	Pc
a/Å	10.9994(4)
b/Å	10.9593(4)
c/Å	38.7750(14)
α/°	90
β/°	90.115(6)
γ/°	90
Volume/Å^3	4674.2(3)
Z	4
ρ_{calc}g/cm^3	1.191
μ/mm^{-1}	0.524
F(000)	1776.0
Crystal size/mm^3	0.12 × 0.06 × 0.04
Radiation	CuKα (λ = 1.54178)
2Θ range for data collection/°	8.038 to 128.286
Index ranges	$-12 \le h \le 12$, $-12 \le k \le 12$, $-45 \le l \le 44$
Reflections collected	28597
Independent reflections	13608 [R_{int} = 0.0844, R_{sigma} = 0.1106]
Data/restraints/parameters	13608/2/1189
Goodness-of-fit on F^2	1.035
Final R indexes [I>=2σ (I)]	R_1 = 0.0843, wR_2 = 0.2107
Final R indexes [all data]	R_1 = 0.1141, wR_2 = 0.2310
Largest diff. peak/hole / e Å^{-3}	0.35/-0.29
Flack parameter	0.2(6)

Table S2. Crystal data and structure refinement for **DSBN.**

Compound	DSBN
Empirical formula	$C_{80}H_{87}BN_2O_4$
Chemical formula weight	1151.418
CCDC number	2464390
Temperature/K	170
Crystal system	monoclinic
Space group	$P2_1/c$
a/Å	14.2644(4)
b/Å	17.5784(5)
c/Å	26.3039(7)
α/°	90
β/°	98.416(1)
γ/°	90
Volume/Å^3	6524.6(3)
Z	4
ρ_{calc}g/cm^3	1.172
μ/mm^{-1}	0.070
F(000)	2473.3
Crystal size/mm^3	0.11 × 0.05 × 0.03
Radiation	MoKα (λ = 0.71073)
2Θ range for data collection/°	3.86 to 52.8
Index ranges	$-17 \le h \le 17$, $-21 \le k \le 21$, $-32 \le l \le 32$
Reflections collected	50332
Independent reflections	13328 [R_{int} = 0.0736, R_{sigma} = 0.0664]
Data/restraints/parameters	13328/0/688
Goodness-of-fit on F^2	1.0461
Final R indexes [I>=2σ (I)]	R_1 = 0.0446, wR_2 = 0.1126
Final R indexes [all data]	R_1 = 0.0709, wR_2 = 0.1262
Largest diff. peak/hole / e Å^{-3}	0.32/-0.30

Table S3. Crystal data and structure refinement for **DSBNS.**

Compound	DSBNS
Empirical formula	$C_{77}H_{76}BN_2O_{2.5}S$
Chemical formula weight	1112.26
CCDC number	2464393
Temperature/K	170
Crystal system	triclinic
Space group	P-1
a/Å	12.865(3)
b/Å	14.573(3)
c/Å	18.248(4)
α/°	88.548(15)
β/°	72.501(13)
γ/°	71.849(13)
Volume/Å^3	3091.5(11)
Z	2
ρ_{calc}g/cm^3	1.195
μ/mm^{-1}	0.847
F(000)	1186.0
Crystal size/mm^3	0.09 × 0.03 × 0.02
Radiation	CuKα (λ = 1.54178)
2Θ range for data collection/°	5.092 to 128.16
Index ranges	$-13 \leq h \leq 14$, $-16 \leq k \leq 16$, $-21 \leq l \leq 20$
Reflections collected	33711
Independent reflections	9945 [R_{int} = 0.0900, R_{sigma} = 0.0869]
Data/restraints/parameters	9945/132/753
Goodness-of-fit on F^2	1.068
Final R indexes [I>=2σ (I)]	R_1 = 0.0951, wR_2 = 0.2309
Final R indexes [all data]	R_1 = 0.1483, wR_2 = 0.2570
Largest diff. peak/hole / e Å^{-3}	0.33/-0.33

5. Theoretical calculations

Theoretical calculations were performed by the Gaussian 09 program package, density functional theory (DFT) and time-dependent DFT (TD-DFT) calculations were performed at the B3LYP/6-31G(d,p) level. Based on the single-crystal structures and optimized geometric configurations, the energy levels, the dihedral angles of these molecules, the highest occupied molecular orbital (HOMO), and the lowest unoccupied molecular orbital (LUMO), as well as natural transition orbitals (NTO) and RMSD were obtained logically.

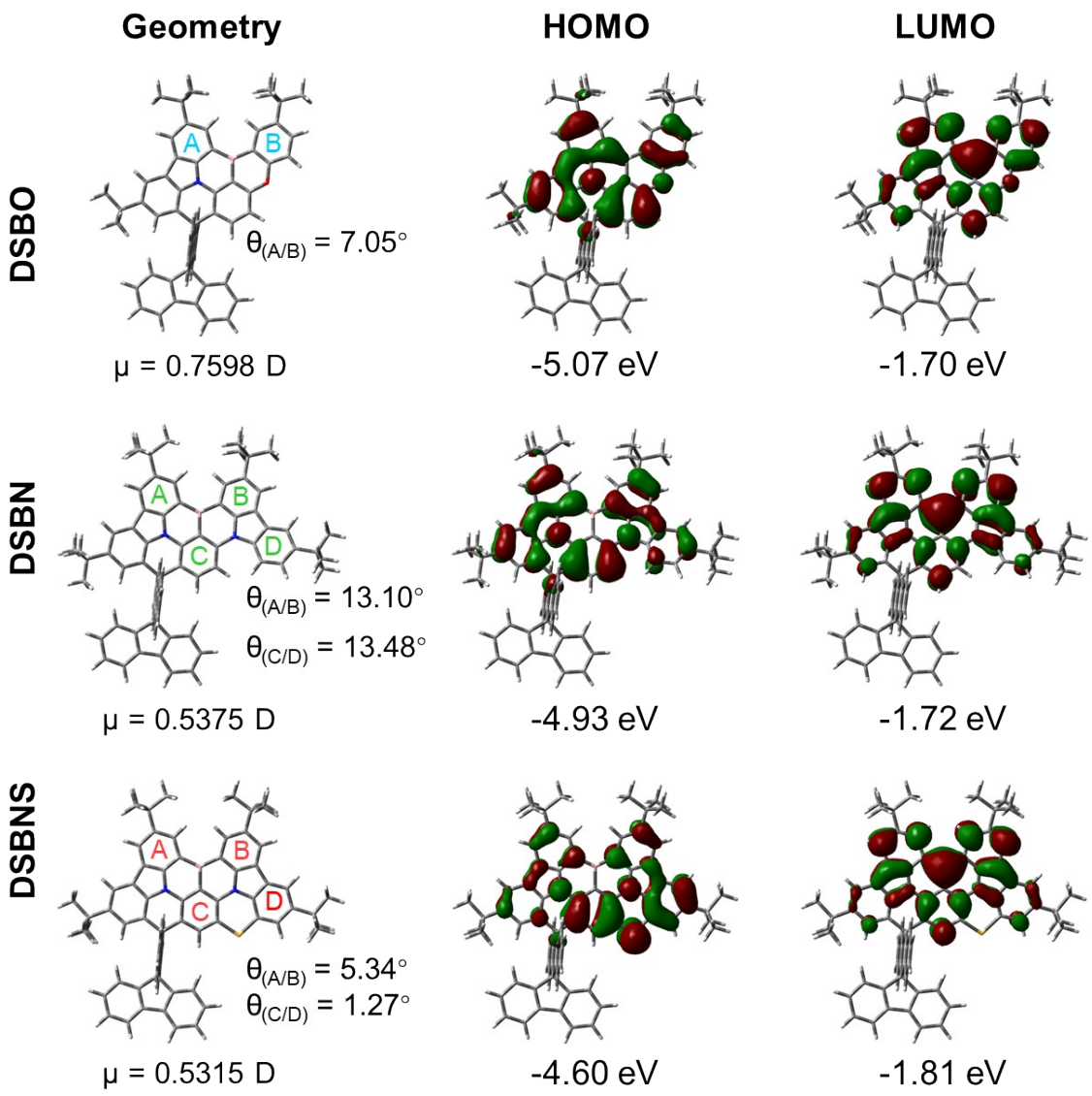

Figure S13. Molecular geometries, dihedral angels, dipole moments, HOMO/LUMO distributions and HOMO–LUMO energy levels of DSBO, DSBN and DSBNS.

6. Photophysical Characterization

Perkin-Elmer Lambda 750 UV-Vis spectrophotometer was applied to record UV-vis spectra at 25 °C. Photoluminescence (PL) spectra were determined on a FM-4 type fluorescence spectrophotometer (JY company, French) at 25 °C. Phosphorescence spectra (Phos) were recorded on the FLS 920 spectrometer (Einburgh Corporation) at 77 K. The transient PL decay curves were obtained by Quantaurus-Tau fluorescence lifetime spectrometer (C11367-32 and FLS980) under a vacuum atmosphere. The photoluminescence quantum yields (PLQYs) were achieved by a C9920-02G type fluorescence spectrophotometer (HAMAMASTU, Japan), the integrating sphere was purged with dry argon to maintain an inert atmosphere.

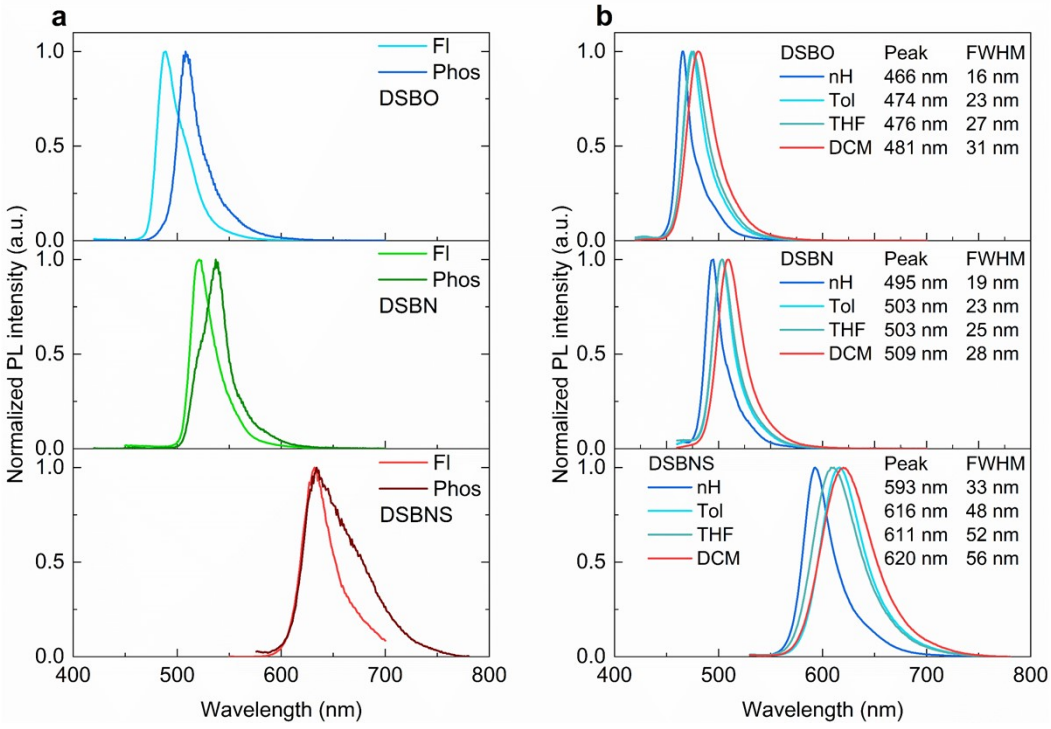

Figure S14. (a) Low-temperature fluorescence and phosphorescence spectra of DSBO, DSBN and DSBNS in toluene at 77 K. (b) Room-temperature PL spectra of DSBO, DSBN and DSBNS in various solvents. (nH=*n*-hexane, Tol=toluene, Diox=1,4-Dioxane THF= tetrahydrofuran, DCM=dichloromethane. Ex: 400 nm).

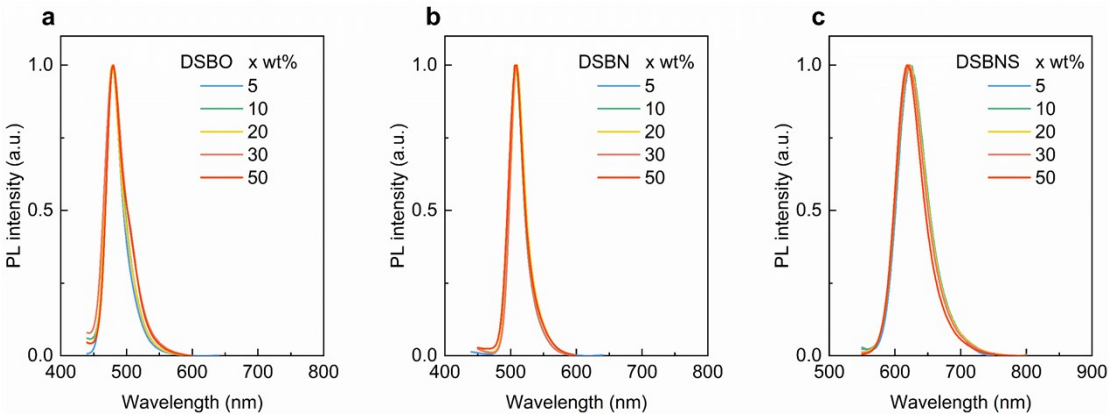

Figure S15. PL spectra with various doping concentrations of 5-50 wt%.

Analysis of Rate Constants: The rate constants of radiative decay ($k_{r,S}$) and nonradiative decay ($k_{nr,S}$) from S_1 to S_0 states, the rate constants of intersystem crossing (k_{ISC}) and reverse intersystem crossing (k_{RISC}) were calculated from the following six equations:

$$k_p = 1/\tau_p \quad \text{Eq.(1)}$$

$$k_d = 1/\tau_d \quad \text{Eq.(2)}$$

$$k_{r,S} = \Phi_p k_p + \Phi_d k_d \approx \Phi_p k_p \quad \text{Eq.(3)}$$

$$k_{nr,S} = \frac{1 - \Phi_{PL}}{\Phi_{PL}} k_{r,S} \quad \text{Eq.(4)}$$

$$k_{ISC} = k_p - k_{r,S} - k_{nr,S} \quad \text{Eq.(5)}$$

$$k_{RISC} = (k_p k_d \Phi_d)/(k_{ISC} \Phi_p) \quad \text{Eq.(6)}$$

Where τ_p and τ_d represent the prompt and decay fluorescence lifetime, which determined from transient PL spectra. The k_p and k_d represent the decay rate constants for prompt and delayed fluorescence, respectively. Φ_p and Φ_d indicate prompt and delayed fluorescence components and can be distinguished from the total Φ_{PL} by comparing the integrated intensities of prompt and delayed components in the transient PL spectra.

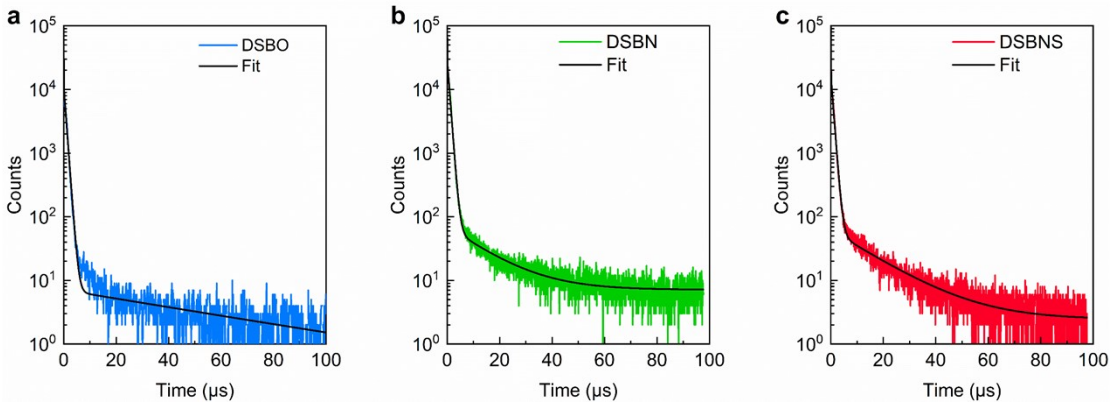

Figure S16. Transient photoluminescence decay curves of 5 wt%-doped films.

Table S4. Photophysical characteristics of DSBO, DSBN and DSBNS in doped films.

Film[a]	Φ_p [%][b]	Φ_d [%][b]	τ_p [ns][c]	τ_d [μs][c]	k_r [10^7 s^{-1}][d]	k_{nr} [10^6 s^{-1}][e]	k_{ISC} [10^7 s^{-1}][f]	k_{RISC} [10^5 s^{-1}][g]
DSBO	20	78	5.9	62.7	3.4	0.7	13.6	0.8
DSBN	13	86	3.7	14.2	3.4	0.3	23.6	5.6
DSBNS	22	77	10.1	16.6	2.2	0.2	7.7	2.7

[a] The doped films are 5 wt% DSBO-doped mCBP, 5 wt% DSBN-doped mCBP and 5 wt% DSBN-doped DMIC-TRZ.

[b] Quantum yields for prompt fluorescence (Φ_p) and delayed fluorescence (Φ_d) for the neat film, $\Phi_p + \Phi_d = \Phi_{PL}$.

[c] Lifetime of the prompt component (τ_p) and delayed component (τ_d) as determined from the transient PL.

[d] Radiative rate constants of S_1, $k_r = \Phi_p/\tau_p + \Phi_d/\tau_d$.

[e] Nonradiative rate constants of S_1, $k_{nr} = k_r(1 - \Phi_{PL})/\Phi_{PL}$.

[f] Rate constants for ISC ($S_1 \rightarrow T_1$), $k_{ISC} = k_p - k_r - k_{nr}$.

[g] Rate constants for RISC ($T_1 \rightarrow S_1$), $k_{RISC} = k_p k_d / k_{ISC} \cdot \Phi_d/\Phi_p$.

7. Device Fabrication and Measurement

To evaluate the EL performance of DSBO, DSBN and DSBNS as emitter materials, we fabricated multilayered TADF OLEDs. The ITO coated glass substrates with a sheet resistance of 15 Ω square^{-1} were ultrasonic cleaned with acetone/ethanol and dried with nitrogen gas flow, followed by 20 min ultraviolet light-ozone (UVO) treatment in a UV-ozone surface processor (PL16 series, Sen Lights Corporation). Then the sample was transferred to the deposition system. All organic layers were deposited at a rate of 1 Å s^{-1}, and subsequently LiF was deposited at 0.1 Å s^{-1} and then capped with Al (ca. 5 Å s^{-1}) through a shadow mask in a vacuum of 2×10^{-5} mbar. For all the devices, the emitting areas were determined by the overlap of two electrodes as 10 mm^2. The as-fabricated devices were measured in ambient environment without any encapsulation. Current density-voltage-luminance (J-V-L) characteristics and EL spectra of the devices were measured simultaneously with a source meter (Keithley model 2400) and a luminance meter/spectrometer (PhotoResearch PR670). The CIE 1931 colour coordinates were obtained from the EL spectra. The EQE values were calculated by assuming an ideal Lambertian emission profile, which was verified by the independent measurements of luminous flux with an integrating sphere (Hamamatsu Photonics K.K. C9920-12).

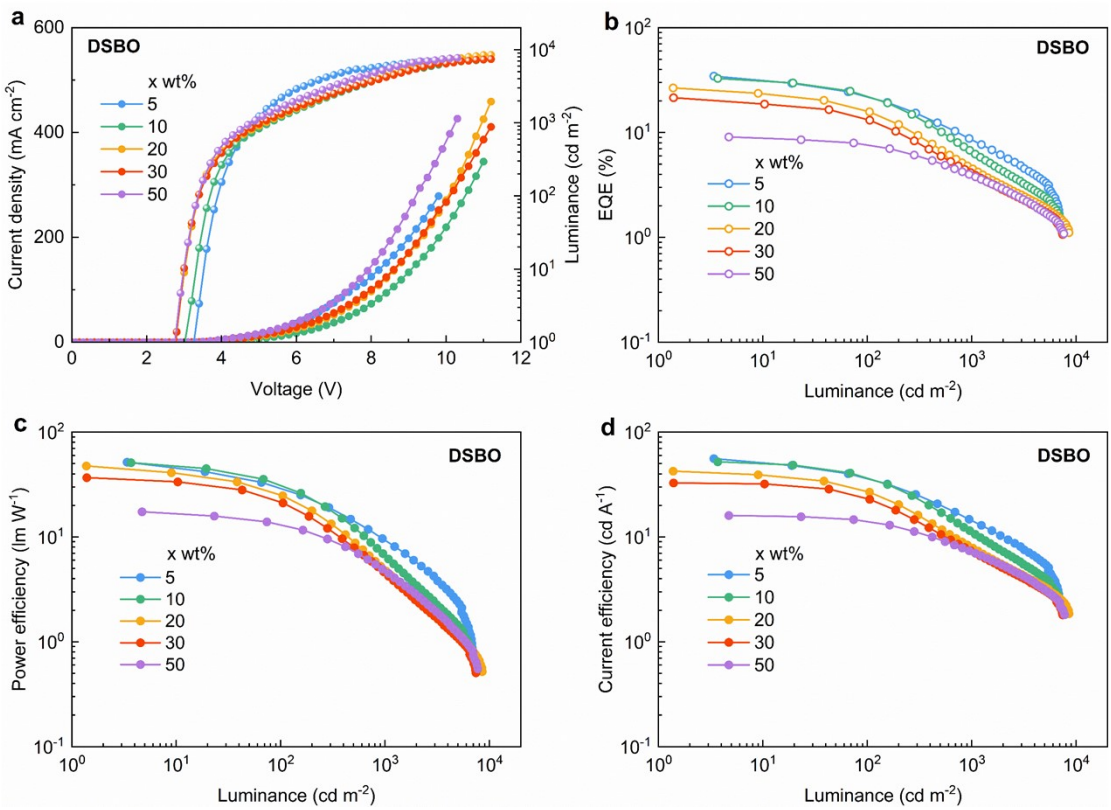

Figure S17. EL performance of DSBO-based devices. a) Current density-voltage-luminance (J-V-L) characteristics. b) EQE-luminance curves. c) Power efficiency versus luminance characteristics. d) Current efficiency versus luminance characteristics.

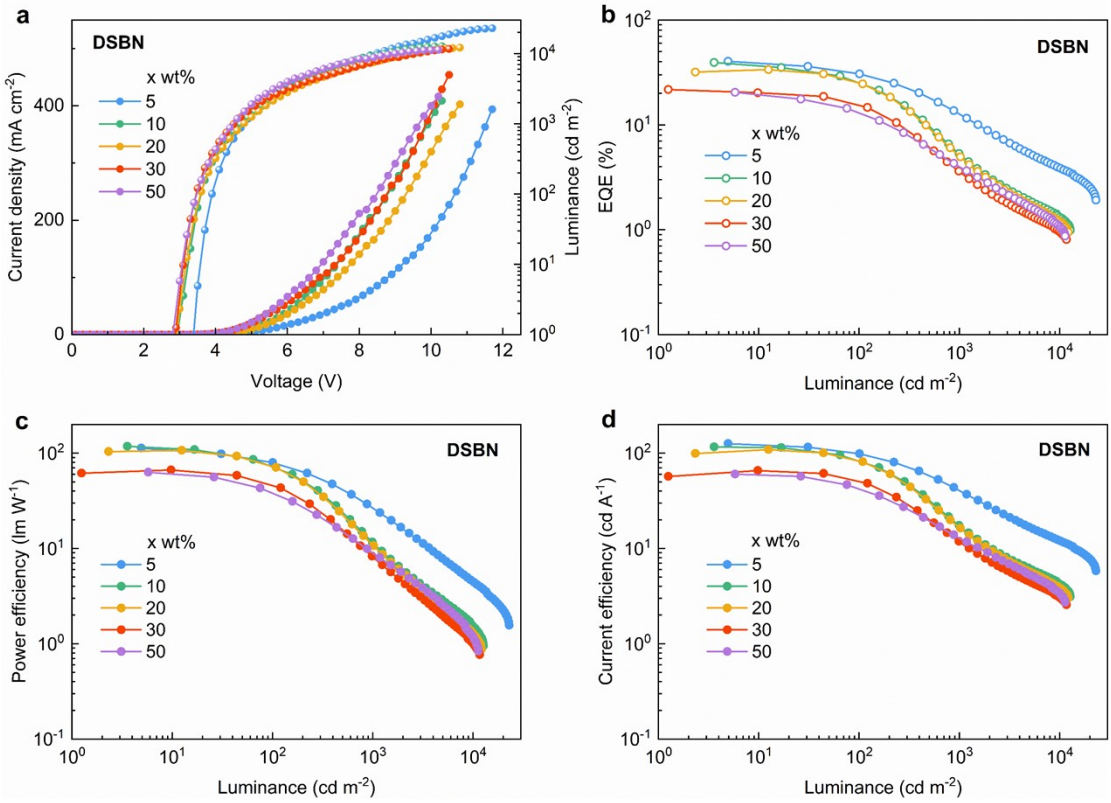

Figure S18. EL performance of DSBN-based devices. a) Current density-voltage-luminance (J-V-L) characteristics. b) EQE-luminance curves. c) Power efficiency versus luminance characteristics. d) Current efficiency versus luminance characteristics.

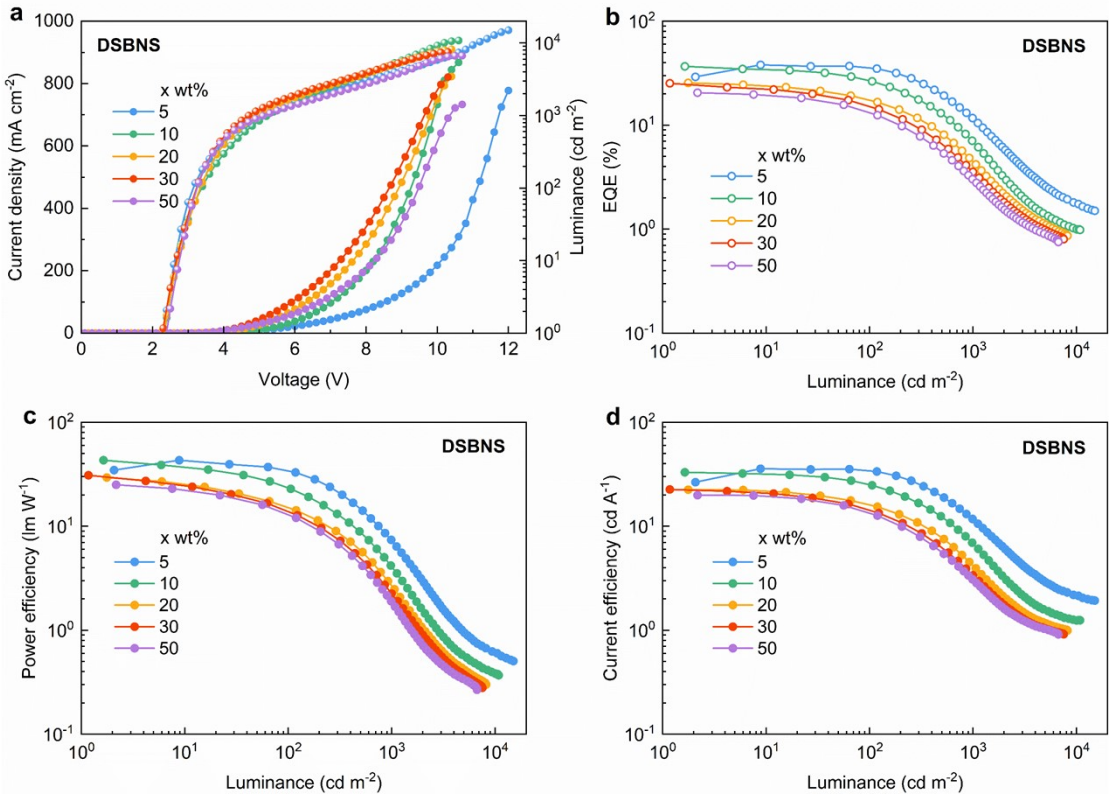

Figure S19. EL performance of DSBNS-based devices. a) Current density-voltage-luminance (J-V-L) characteristics. b) EQE-luminance curves. c) Power efficiency versus luminance characteristics. d) Current efficiency versus luminance characteristics.

Table S5. Summary of the EL data.

Emitter	x [wt%]	V_{on}[a] [V]	L_{max}[b] [cd m^{-2}]	EQE_{max}[c] [%]	PE_{max}[c] [lm W^{-1}]	CE_{max}[c] [cd A^{-1}]	λ_{EL}[d] [nm]	FWHM[d] [nm]	CIE[d] (x, y)
DSBO	5	3.3	6890	34.5	51.7	55.9	480	28	(0.13, 0.30)
	10	3.1	7304	32.8	51.1	52.1	480	28	(0.12, 0.31)
	20	2.8	8508	26.6	47.6	42.4	480	28	(0.12, 0.32)
	30	2.8	7419	21.5	36.7	32.7	480	28	(0.12, 0.33)
	50	2.8	7732	9.1	17.3	16.0	480	28	(0.13, 0.33)
DSBN	5	3.4	22870	40.4	112.8	125.7	510	25	(0.13, 0.71)
	10	3.0	12680	39.4	117.8	116.2	510	25	(0.14, 0.71)
	20	2.9	12130	31.9	103.7	99.0	510	25	(0.14, 0.71)
	30	2.9	11620	21.7	61.5	56.8	510	25	(0.14, 0.71)
	50	2.9	11260	19.9	66.9	61.7	510	24	(0.15, 0.70)
DSBNS	5	2.4	15020	38.0	43.1	35.7	628	58	(0.67, 0.32)
	10	2.4	10820	36.7	43.2	33.0	628	58	(0.67, 0.32)
	20	2.4	8190	25.5	29.4	25.5	628	58	(0.67, 0.32)
	30	2.4	7524	25.3	30.9	22.6	628	57	(0.68, 0.32)
	50	2.4	6685	20.5	19.9	20.5	628	54	(0.68, 0.32)

[a] Turn-on voltage (V_{on}) at 1 cd m^{-2}. [b] Maximum luminance. [c] EQE, CE and PE at maximum. [d] EL peak, FWHM and CIE coordinates.

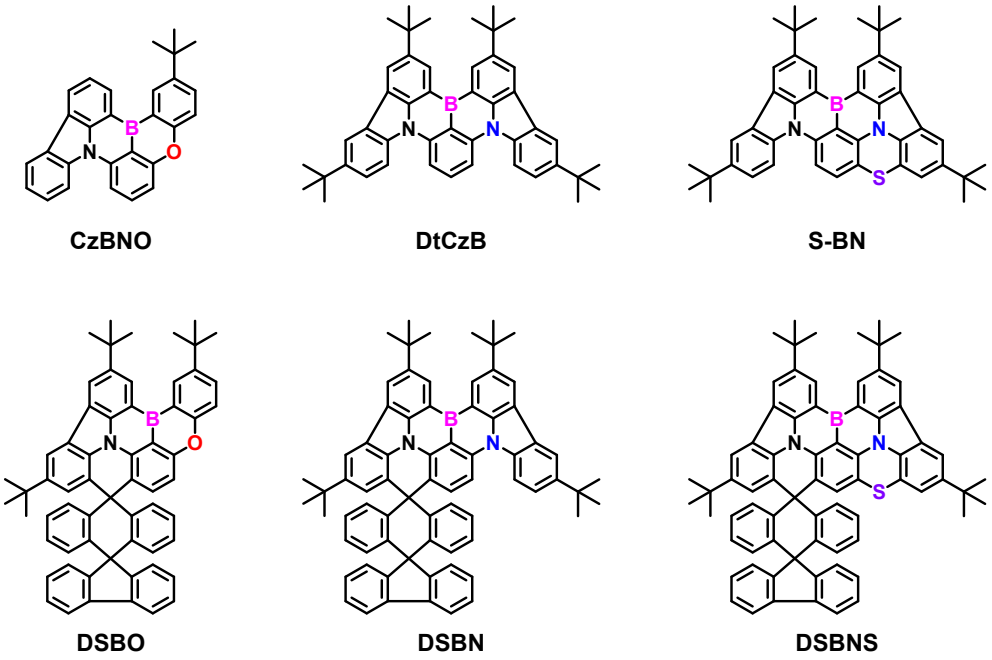

Figure S20. The chemical structure of planar and orthogonal di-spiro MR-TADF compounds.

Table S6. Comparative EL data for planar and orthogonal di-spiro MR-TADF emitters.

Emitter	EQE_{max} [%]	PE_{max} [lm W^{-1}]	CE_{max} [cd A^{-1}]	λ_{EL} [nm]	FWHM [nm]	CIE (x, y)
CzBNO	13.6	—	14.7	454	36	(0.14, 0.08)
DSBO	34.5	51.7	55.9	480	28	(0.13, 0.30)
DtCzB	23.2	42.3	40.4	488	27	(0.10, 0.35)
DSBN	40.4	112.8	125.7	510	25	(0.13, 0.71)
S-BN	39.9	93.6	74.5	600	58	(0.61, 0.39)
DSBNS	38.0	43.1	35.7	628	58	(0.67, 0.32)